Feedforward Control of the Rate-Dependent Viscoelastic Hysteresis Nonlinearity in Dielectric Elastomer Actuators

Jiang Zou and Guoying Gu

***Abstract*—Dielectric elastomer actuators have shown promising applications in the field of soft robotics. However, due to their rate-dependent viscoelastic hysteresis nonlinearity, it is still challenging to achieve precision tracking control of dielectric elastomer actuators. In this letter, we propose a feedforward control approach that can compensate for the rate-dependent viscoelastic hysteresis nonlinearity with maximum tracking errors of 6.18% and root-mean-square errors of 2.96% when the frequency of the input voltage is between 0.05 Hz and 1.5 Hz. Our control approach consists of two feedforward compensators: 1) for the ease of the hysteresis compensation, a creep compensator is firstly developed to remove the viscoelastic creep nonlinearity; 2) based on a phenomenological mathematical model, an inverse hysteresis compensator is then developed to compensate for the rate-dependent viscoelastic hysteresis nonlinearity. Experimental results of tracking various periodic trajectories demonstrate that: the maximum tracking errors are reduced by 87.17% and the root-mean-square errors are decreased by 89.53%, by comparing the results without the viscoelastic compensation. It is the first time to successfully compensate for both the viscoelastic creep nonlinearity and rate-dependent hysteresis nonlinearity of dielectric elastomer actuators by a feedforward control approach, which may pave the way for further applications in dielectric-elastomer-actuators based soft robotics.**

***Index Terms*—Soft material robotics, motion control, dynamics.**

I. Introduction

DUE to their high energy density, large deformation and fast response speed [1], dielectric elastomer actuators have been widely adopted as soft actuation technology to actuate soft robotics, such as climbing robots [2], humanoid robots [3]–[6], crawling robots [7]–[11], swimming robots [12]–[14] and gripping robots [15]–[17]. However, accurate tracking control of dielectric elastomer actuators is still an open problem. The main challenge lies in their inherent nonlinear viscoelasticity that usually causes viscoelastic creep and hysteresis nonlinearities [18]–[20]. In general, the viscoelastic creep nonlinearity is a slow-time drift phenomenon and many controll approaches have been developed to remove it [21], [22]. However, there is still lack of effective approaches for viscoelastic hysteresis compensation, because the viscoelastic hysteresis nonlinearity is non-smooth, asymmetric and rate-dependent [23]–[25].

Whilst many efforts have been made to design controllers for dielectric elastomer actuators, such as feedforward controllers [21], [26] and sensorless feedback controllers [22], [27], they mainly use to eliminate super-elastic nonlinearity. Therefore, tracking step trajectory is usually adopted for the controllers' verification, may not effective for the periodic trajectory, without considering the viscoelastic hysteresis nonlinearity. Recently, some control approaches, such as adaptive radial basis function neural network sliding model control [28], adaptive sliding model control [29] and nonlinear PID control [30], [31] have been developed for the viscoelastic compensation. However, those controllers are either effective at specific frequency or not verified by experiments. In addition, a direct inverse hysteresis compensation method [20] has been introduced to remove the rate-independent hysteresis nonlinearity of the dielectric elastomer actuator, but it can't compensate for rate-dependent hysteresis nonlinearity. To our knowledge, development of an effective control approach for the asymmetric and rate-dependent viscoelastic hysteresis compensation of dielectric elastomer actuators has not been achieved.

Here, we propose a feedforward control approach for high-precision periodic trajectory tracking of a dielectric elastomer actuator. Our feedforward control approach is developed with two cascaded compensators. Firstly, to avoid external sensor, we adopt a feedforward creep compensator with an identified creep model to compensate for the viscoelastic creep nonlinearity. The experimental results of tracking the step trajectories demonstrate that the creep nonlinearity is limited to 2%, which is reduced by 66.67%. Then, another inverse hysteresis compensator with a modified rate-dependent Prandtl-Ishlinskii model is designed to mitigate the asymmetric and rate-dependent viscoelastic hysteresis nonlinearity of the creep-compensated dielectric elastomer actuator. The experimental results show that the maximum tracking errors and root-mean-square errors of tracking sinusoidal trajectories are less than 6.18% and 2.96%, respectively, when the frequencies of the trajectories are within the range of 0.05 Hz to 1.5 Hz. By comparing to the results without our

Manuscript received September 10, 2018; accepted January 30, 2019. Date of publication March 4, 2019; date of current version March 15, 2019. This letter was recommended for publication by Associate Editor L. Wen and Editor K.-J. Cho upon evaluation of the reviewers' comments. This work was supported in part by the National Natural Science Foundation of China under Grants 51622506 and 51620105002 and in part by the Science and Technology Commission of Shanghai Municipality under Grant 16JC1401000. *(Corresponding author: Guoying Gu.)*

The authors are with the Soft Robotics and Biodesign Lab, Robotics Institute, School of Mechanical Engineering, Shanghai Jiao Tong University, Shanghai 200240, China, and also with the State Key Laboratory of Mechanical System and Vibration, Shanghai Jiao Tong University, Shanghai 200240, China (e-mail: sj_ustb@sjtu.edu.cn; guguoying@sjtu.edu.cn).

Digital Object Identifier 10.1109/LRA.2019.2902954

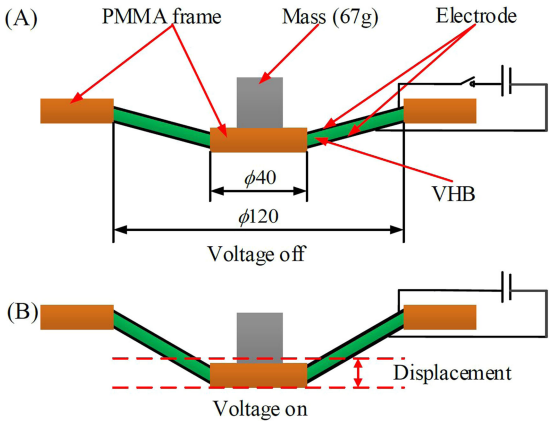

Fig. 1. Working principle of the conical dielectric elastomer actuator. (A) Voltage off. (B) Voltage on.

compensators, the maximum tracking errors and the root-mean-square errors are reduced by 87.17% and 89.53%, respectively. Therefore, our control approach successfully compensates for both viscoelastic creep and rate-dependent viscoelastic hysteresis nonlinearities of the dielectric elastomer actuator. The main contribution of this work depends on the fact that it is the first time to achieve tracking control of dielectric elastomer actuators by compensating for creep nonlinearity and rate-dependent viscoelastic hysteresis nonlinearity.

The structure of this letter can be summarized as follow. Section II includes the fabrication of the dielectric elastomer actuator, experimental setup and experimental phenomena. Section III provides the modeling and compensating approach for the viscoelastic creep nonlinearity. The modeling and compensating approaches for the asymmetric and rate-dependent viscoelastic hysteresis nonlinearity are detailed in Section IV and Section V presents the conclussion of this letter.

II. System Description

A. Fabrication of the Conical Dielectric Elastomer Actuator

In this work, we adopt a conical dielectric elastomer actuator for proof-of-concept testing. To fabricate the actuator, four steps are involved: i) a dielectric elastomer membrane (3M VHB 4905, thickness 0.5 mm) is bi-directionally pre-stretched by three times; ii) an outer and inner stiff frames (acrylic board, thickness 3 mm) are adopted to support the pre-stretched dielectric elastomer membrane; iii) both sides of the pre-stretched dielectric elastomer membrane are covered by carbon grease (MG Chemical 846-80G) based compliant electrodes; iv) in order to generate a vertical linear movement, a mass (67 g) is applied to the center of the conical dielectric elastomer actuator. Fig. 1 shows the working principle of the conical dielectric elastomer actuator. We should note that the breakdown voltage of our actuator [20], [21] is about 4 kV and the minimum actuated voltage is about 0.5 kV. Therefore, the exciting voltage is limited between 0.5 kV and 3.5 kV in this work. In addition, when the step voltage of 3.5 kV is applied, the maximum displacement of the actuator is about 4 mm, which equals to about 16.62% area strain range.

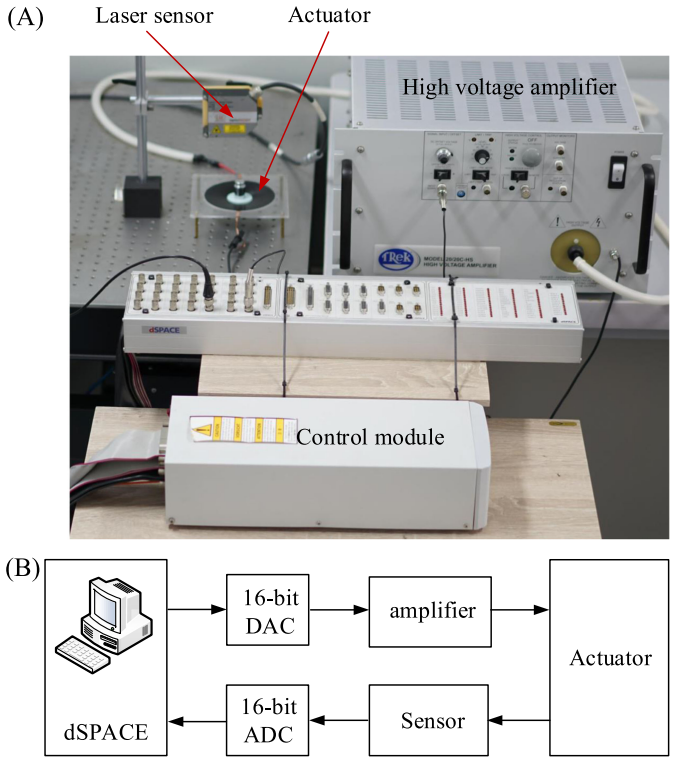

Fig. 2. The whole experimental setup. (A) Experimental platform. (B) Block diagram.

B. Experimental Setup

Fig. 2A shows the experimental setup that is used to investigate the viscoelastic nonlinearity of the dielectric elastomer actuator and verify the effectiveness of the viscoelatic compensators. The high voltage amplifier (TREK 20/20C-HS, TREK INC., NY, USA) with a fixed gain of 2000 is used to generate high voltages for the dielectric elastomer actuator. The laser sensor (Micro-Epsilon ILD2300-100, range of 100 mm, Micro-Epsilon, Ortenburg, Germany) is utilized to record the real-time displacement of the dielectric elastomer actuator. The control module (dSPACE-DS1103, dSPACE, Paderborn, Germany) is used to control the high voltage amplifier and capture the displacement signal from the laser sensor. In this work, the sampling time equals to 1 ms. Fig. 2B shows a block diagram of the whole experimental setup.

C. Characterization of the Viscoelastic Nonlinearity

In this section, we firstly conduct a series of experiments to characterize the viscoelastic response of the dielectric elastomer actuator. In order to capture the rate-dependent behavior of the viscoelastic hysteresis nonlinearity, sinusoidal exciting voltages with different frequencies (f = 0.05 Hz, 0.25 Hz, 0.5 Hz, 0.75 Hz, 1.0 Hz, 1.25 Hz and 1.5 Hz, Fig. 3A) are adopted to drive the conical dielectric elastomer actuator. Fig. 3B shows

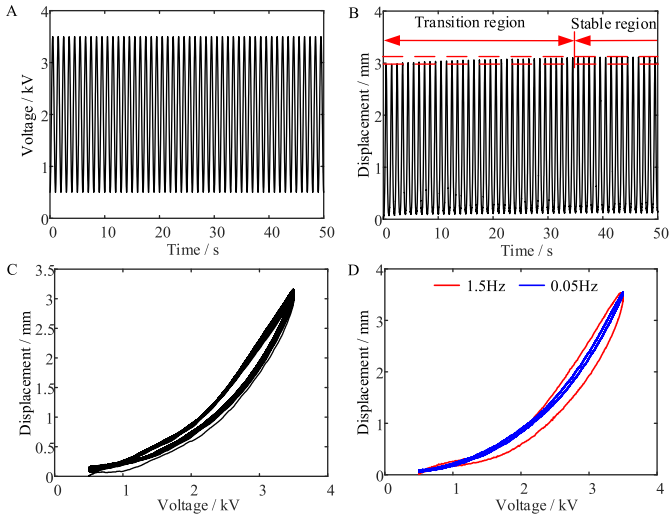

Fig. 3. The viscoelastic response of the conical dielectric elastomer actuator. (A) The input sinusoidal voltage with a frequency of 1 Hz is plotted as a function of time. (B) The corresponding displacement of the actuator under the sinusoidal exciting voltage in (A) is plotted as a function of time. (C) The displacement is plotted as a function of the input voltage when the frequency equals to 1 Hz. (D) The hysteresis loops under two different frequencies.

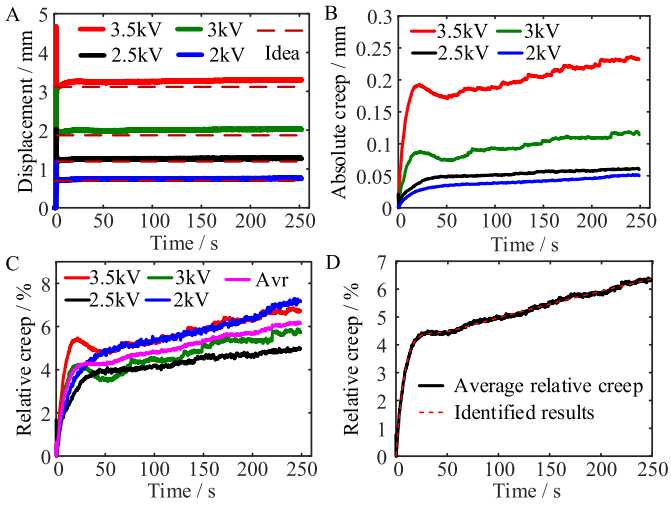

Fig. 4. Modeling the viscoelastic creep nonlinearity of the conical dielectric elastomer actuator. (A) Step responses of the actuator under different step voltages are plotted as a function of time. (B) Absolute creep responses are plotted as a function of time. (C) Relative creep responses are plotted as a function of time. (D) Comparison of experimental data and identified model.

one example of the experimental results in the time domain when the input frequency is 1 Hz, meanwhile, the displacement is also plotted as a function of input voltage shown in Fig. 3C. In addition, Fig. 3D shows the comparisons of viscoelastic hysteresis loops between two frequencies (0.05 Hz and 1.5 Hz). From the experimental results, we can observe that:

i) The viscoelastic response of the actuator can be separated into two regions in the time domain, including transition region and stable region (Fig. 3B). During the transition region, there is an obvious drift phenomenon called viscoelastic creep nonlinearity. It lasts about 33 seconds and then becomes ignorable during the stable region, which can also be shown in the hysteresis loops (Fig. 3C).

ii) The viscoelastic hysteresis nonlinearity is both asymmetric and rate-dependent (Fig. 3D). When the frequency of the input voltage changes from 0.05 Hz to 1.5 Hz, the width of the viscoelastic hysteresis loop increases by about 320% while the amplitude of them almost keeps constant.

The above observations indicate that: i) during the transition region, the viscoelastic hysteresis nonlinearity and viscoelastic creep nonlinearity are coupled; ii) during the stable region, the viscoelastic hysteresis nonlinearity is dominant and the viscoelastic creep nonlinearity can be ignored. Therefore, we will first develop a feedforward creep compensator for removing the drift phenomenon, and then design an inverse hysteresis compensator for the creep-compensated actuator to mitigate the asymmetric and rate-dependent hysteresis nonlinearity, which will be detailed in the following sections.

Remark: We should mention that: due to the actuators' natural frequency equals to about 3 Hz [20], the maximum input frequency of the input voltage doesn't exceed 1.5 Hz.

III. Creep Compensation

To remove viscoelastic creep effect, a relative creep model [21] is identified to describe the creep effect, which is then used to construct the feedforward creep compensator.

A. Viscoelastic Creep Description

To reveal the responses of viscoelastic creep nonlinearity, we firstly conduct the tests on the conical dielectric elastomer actuators with different step voltages. Due to the breakdown voltage of the dielectric elastomer actuator is about 4 kV, the maximum amplitude of the step voltage is limited to 3.5 kV. In addition, the minimum step voltage is set to be 2 kV for the clear observation of the moving displacement. Therefore, we select four step voltages as 2 kV, 2.5 kV, 3 kV and 3.5 kV to excite the conical dielectric elastomer actuator. Based on the experimental results (Fig. 4A), we can see that the step responses can be separated into two regions: dynamical region and creep region. The vibration dominates the dynamical region and lasts about one second. Considering that the purpose is to eliminate the viscoelastic creep nonlinearity, we only take the experimental data in creep region into account.

For the convenience of description, we define an idea displacement $D_I(t)$ as the displacement at the separated time of the two region. In this work, the separated time equals to 1 second. The differences between real output displacement $D_R(t)$ and the $D_I(t)$ are defined as absolute creep displacement $D_C(t)$. Fig. 4B shows the comparisons of $D_C(t)$ among different voltages $V(t)$, which demonstrate that $D_C(t)$ highly depends on the amplitudes of $V(t)$. Then, we give the definition of the relative creep displacement $C_R(t)$:

$$C_R(t) = \frac{D_R(t) - D_I(t)}{D_I(t)} = \frac{D_C(t)}{D_I(t)} \tag{1}$$

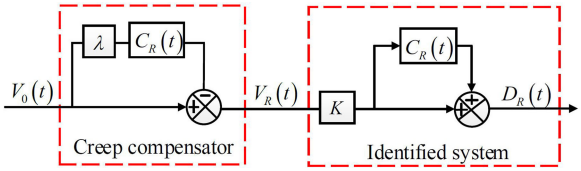

Fig. 5. Block diagram of the creep compensator.

By the introduction of $C_R(t)$, we can see from Fig. 4C that the creep can be considered as independent on the amplitude of $V(t)$. To obtain $C_R(t)$, a system identification approach is adopted, which involves four steps: i) calculating average relative creep displacement based on the experimental data; ii) selecting a continuous-time transfer function as the identification model of $C_R(t)$; iii) using Matlab identification box to identify the parameters in the model; iv) comparing the identification model with the experimental data, if they are not fit well, increasing the model order and repeating the identification process. We finally choose a three-order transfer function as the relative creep model, which can be written as:

$$C_R(t) = \frac{0.499s^2 + 0.058s + 0.000217}{s^3 + 0.199s^2 + 0.0144s + 0.0000149} \tag{2}$$

Fig. 4D shows the comparison between the relative creep model and experimental results, which demonstrates that the identified model can well predict the relative creep response.

B. Viscoelastic Creep Compensation

Based on the identified viscoelastic creep model, a feedforward creep compensator can be developed as [21]:

$$\frac{V_C(t)}{V_0(t)} = [1 - \lambda C_R(t)] \tag{3}$$

where $V_C(t)$ and $V_0(t)$ represent the creep voltage and the input voltage, respectively. $\lambda = 0.3$ is an identified constant ratio. Fig. 5 shows the block diagram of the creep compensator. To verify the effectiveness of the creep compensator, different exciting voltages are adopted and the experimental results are shown in Fig. 6. It can be seen that with the creep compensator, the tracking errors of step trajectories are less than 2% (Fig. 6A and B), which indicate that the relative creep nonlinearity is reduced by 66.67%. We further evaluate the performance of the creep compensator with sinusoidal exciting voltages under different frequencies (0.05 Hz to 1.5 Hz). Fig. 6C shows one example of the time-domain output displacement when the frequency is 1 Hz. It demonstrates that the relative creep nonlinearity of the response (Fig. 3B) under sinusoidal exciting voltage still can be removed by the creep controller.

Remark: It should be noted that we select step voltage for identifying the relative creep model lies in the fact that the reference displacement of the step response is constant, which is much easier to separate the creep response from the dynamical response. As can be seen in Fig. 6C, the developed relative creep model can still be used to remove the viscoelastic creep nonlinearity under sinusoidal exciting voltage, which also demonstrates the generality of the development.

IV. Inverse Viscoelastic Hysteresis Compensation

With the creep compensator, we design a controller to mitigate the asymmetric and rate-dependent viscoelastic hysteresis nonlinearity of the dielectric elastomer actuator. To this end, a modified rate-dependent Prandtl-Ishlinskii model (MRPIM) is firstly developed to characterize the viscoelastic hysteresis of the creep-compensated actuator. Then, a direct inverse hysteresis compensator [32], [33] can be designed with the MRPIM to remedy the viscoelastic hysteresis nonlinearity (Fig. 7).

A. Viscoelastic Hysteresis Description

As shown in Fig. 3C, we can see that the viscoelastic hysteresis nonlinearity of the actuator is both asymmetric and rate-dependent. To describe such kind of nonlinearity, a MRPIM is developed as:

$$V(t) = g_1 D_R^3(t) + g_2 D_R(t) + g_3\sqrt{D_R(t)} + \int_0^R a(r) F_r[D_R(t)]\,dr \tag{4}$$

where g_1, g_2 and g_3 represent three constant, $V(t)$ and $D_R(t)$ are the input voltage and the reference displacement, respectively. $a(r)$ and the r represent a density function and a constant threshold of the rate-dependent play operator $F_r[D_R(t)]$, respectively, that is defined as [23], [33]:

$$\begin{aligned} W(0) &= F_r^h[D_R](0) = f_r^h[D_R(0), V(0)] \\ W(t) &= F_r^h[D_R](t) = f_r^h\left[D_R(t), F_r^h[D_R](t-T)\right] \\ f_r^h[D_R(t), W(t)] &= \max\left\{h_l\left[D_R(t), \dot{D}_R(t)\right] - r, \right. \\ &\qquad \left. \min\left[h_r\left(D_R(t), \dot{D}_R(t)\right), W(t)\right]\right\} \end{aligned} \tag{5}$$

where $\dot{D}_R(t)$ is the velocity of the displacement, $h_l\left[D_R(t), \dot{D}_R(t)\right]$ and $h_r\left[D_R(t), \dot{D}_R(t)\right]$ represent two dynamical envelope functions that rely on both the displacement and its' velocity. Based on our experience and experimental observation, the two dynamical envelope functions can be written as:

$$\begin{aligned} h_l\left[D_R(t), \dot{D}_R(t)\right] &= D_R(t) - \alpha\left|\dot{D}_R(t)\right| \\ h_r\left[D_R(t), \dot{D}_R(t)\right] &= D_R(t) + \beta\left|\dot{D}_R(t)\right| \end{aligned} \tag{6}$$

where α and β represent two constants. To simplify the calculating process, the $\dot{D}_R(t)$ is calculated by $[D_R(t) - D_R(t-T)]/T$, with the sampling time of T.

In general, the upper limit of the integration in (4) is infinite, which makes the parameters' identification challenge. To overcome this challenge, we adopt a discrete form of the MRPIM that can be expressed as:

$$V(t) = g_1 D_R^3(t) + g_2 D_R(t) + g_3\sqrt{D_R(t)} + \sum_{i=1}^{N} a_i F_r[D_R(t)] \tag{7}$$

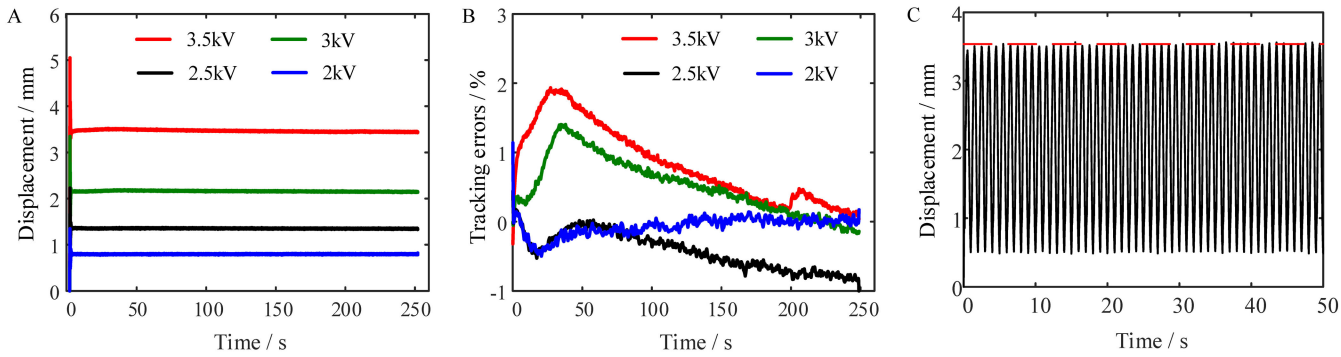

Fig. 6. Experimental results with the creep compensator. (A) Step responses under different step voltages are plotted as a function of time. (B) Tracking errors of step trajectories are plotted as a function of time. (C) The output displacement is plotted as a function of time when the frequency of the periodic exciting voltage equals to 1 Hz.

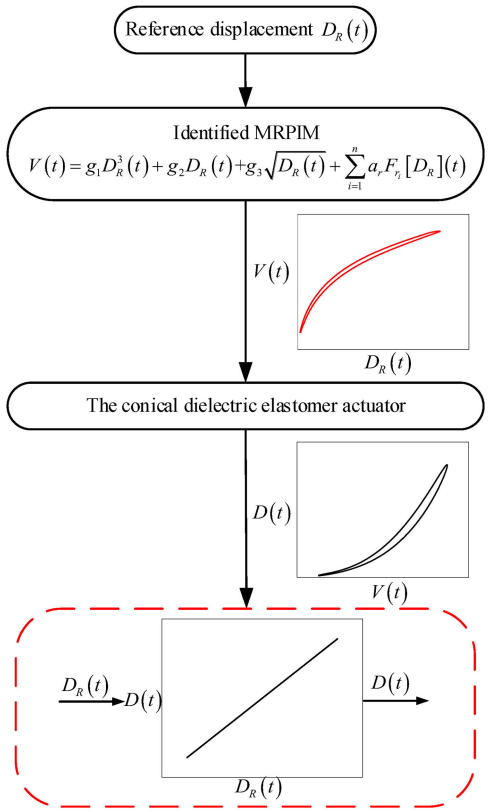

Fig. 7. Flowchart of the inverse hysteresis compensator.

where N is the number of rate-dependent play operators, a_i represents the weighting factor of the ith rate-dependent play operator with a constant threshold value r_i. In the identification, the N is selected as 4, and four constant thresholds r_i equal to 0, 0.2, 0.4 and 0.6, respectively. The rest parameters in (7) are obtained by using a particle swarm optimization algorithm [23], where a fitness function is defined as:

$$F = \min\left\{\sum_{j=1}^{M}\left[\frac{1}{N}\sum_{i=1}^{N}\left(V_{ji}-V_{ji}^{a}\right)^2\right]\right\} \tag{8}$$

To identify the parameters in (7), we randomly select four frequencies in the range of 0.05 Hz to 1.5 Hz. On the

TABLE I
THE IDENTIFIED PARAMETERS OF THE MRPIM

i	r_i	a_i	g_i	α	β
1	0	-0.0335	0.1387	0.0765	1.9784
2	0.2	-8.173e-6	-0.7473		
3	0.4	-1.664e-5	1.7921		
4	0.6	-0.066			

condition of normalized input and output, the model parameters are identified and the identified results are listed on Table I. The comparisons between experimental data and identified results are shown in Fig. 8A, and the identification errors are plotted in Fig. 8B. It can be seen that the model accurately characterizes the asymmetric and rate-dependent viscoelastic hysteresis nonlinearity. In order to quantitatively evaluate the identification accuracy of the MRPIM, the maximum errors e_m and the root-mean-square errors e_{rms} are defined:

$$\begin{aligned} e_m &= \max\frac{|V(i)-V^a(i)|}{\max(V^a)-\min(V^a)} \\ e_{rms} &= \frac{\sqrt{\frac{1}{N}\sum_{i=1}^{N}[V(i)-V^a(i)]^2}}{\max(V^a)-\min(V^a)} \end{aligned} \tag{9}$$

where $V(i)$ and $V^a(i)$ are the predicted results and experimental data, respectively. Then, we can obtain that e_m and e_{rms} are 3.0% and 2.5%, respectively, which clearly demonstrate the effectiveness of the identified model.

B. Direct Inverse Hysteresis Compensation

With the developed MRPIM, we construct an inverse hysteresis compensator cascaded by the creep compensator for the dielectric elastomer actuator (Fig. 9). In order to evluate the performances of the compensator, we conduct series experiments for tracking various sinusoidal trajectories with different frequency. Fig. 10 shows a time-domain example of tracking experimental results when the frequency of the tractory equals to 1 Hz. It can be seen that with the two compensators, the actuator can previsely track sinusoidal trajectory. In addition, Fig. 11 shows the experimental results of tracking various sinusoidal trajectories. In Fig. 11A, the output displacements of the actuator are plotted as a function of the reference displacements under the four frequencies (i.e., 1.5 Hz, 1.0 Hz, 0.5 Hz

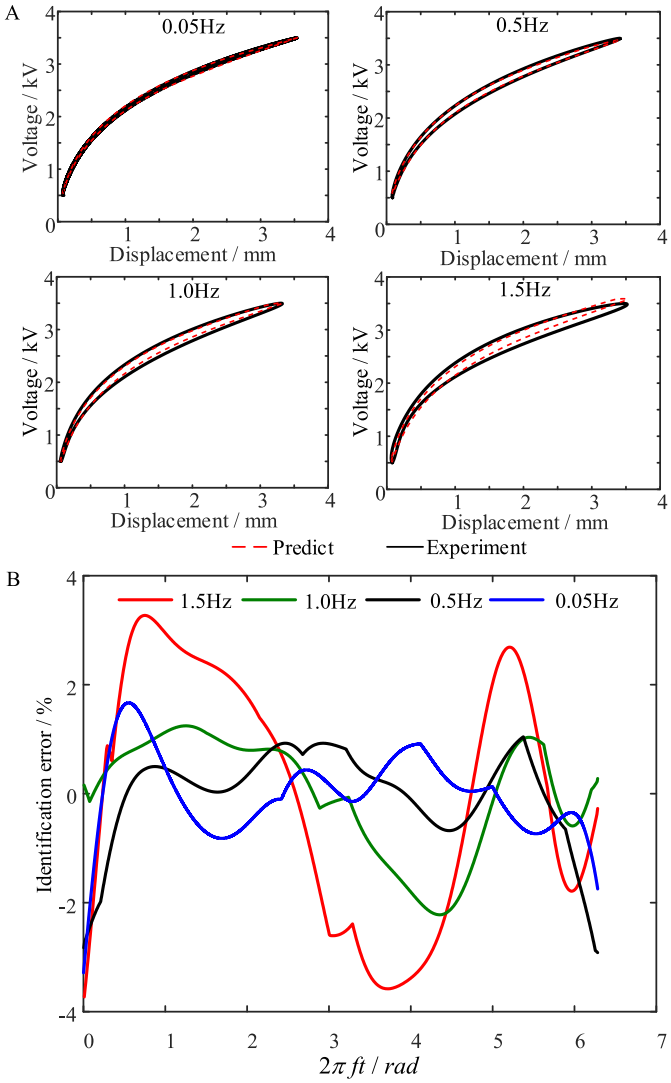

Fig. 8. Identification results with the MRPIM. (A) Comparisons between experimental results and the predicted results from the identified model. (B) Identification errors under different frequencies.

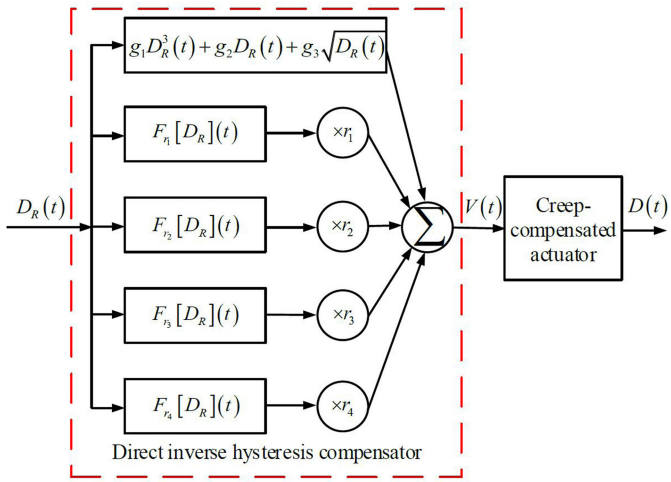

Fig. 9. Block diagram of the direct inverse hysteresis compensator.

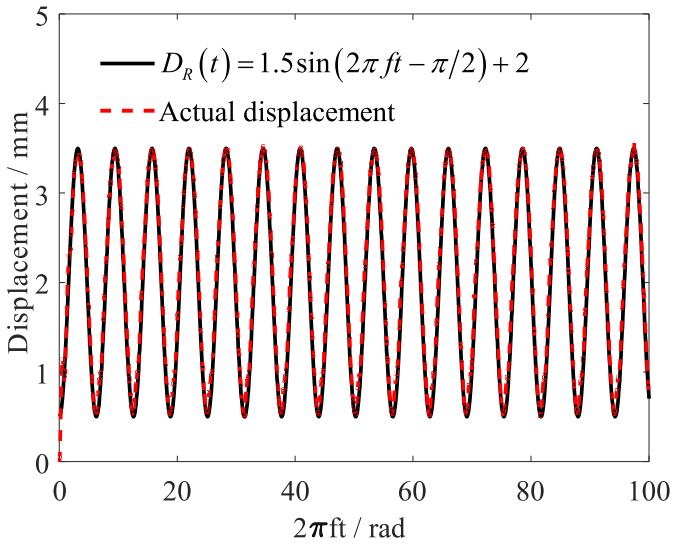

Fig. 10. The reference displacement and actual displacement are plotted as a function of time when the input frequency equals to 1 Hz.

TABLE II
TRACKING ERRORS UNDER DIFFERENT FREQUENCIES

Compensator	Without		Feedforward	
Frequency/Hz	$e_m/\%$	$e_{rms}/\%$	$e_m/\%$	$e_{rms}/\%$
0.05	40.09	25.69	3.42	1.66
0.25	40.52	25.70	3.94	1.84
0.5	41.41	26.08	4.42	2.10
0.75	42.81	26.61	5.25	2.25
1.0	45.01	27.94	5.51	2.54
1.25	45.17	27.62	4.63	2.63
1.5	48.16	28.26	6.18	2.96

and 0.05 Hz), where the asymmetric and rate-dependent viscoelastic hysteresis nonlinearity is well mitigated (by comparing to Fig. 3D). Fig. 11B shows the tracking errors, where both viscoelastic creep and hysteresis nonlinearities are well compensated.

To further evaluate the performance of our control approach, we conduct more experiments for tracking other sinusoidal trajectories with other input frequencies (i.e., 1.25 Hz, 0.75 Hz and 0.25 Hz, different from the frequencies for identification). As shown in Fig. 11C and D, our control approach is also effective to mitigate the viscoelastic creep and rate-dependent hysteresis nonlinearities. The tracking errors of e_m and e_{rms} under different trajectories are summarized in Table II. We can see that with our control approach, e_m and e_{rms} are reduced to 6.18% and 2.96%, respectively. Comparing with the experimental results without our compensators, e_m and e_{rms} are reduced by 87.17% and 89.53%, respectively.

Remark: It should be noted that our modeling approach is phenomenological, which is identified based on the experimental data without taking physical insight into consideration. Without loss of generality, our approach can also be employed to other kinds of dielectric elastomer actuators.

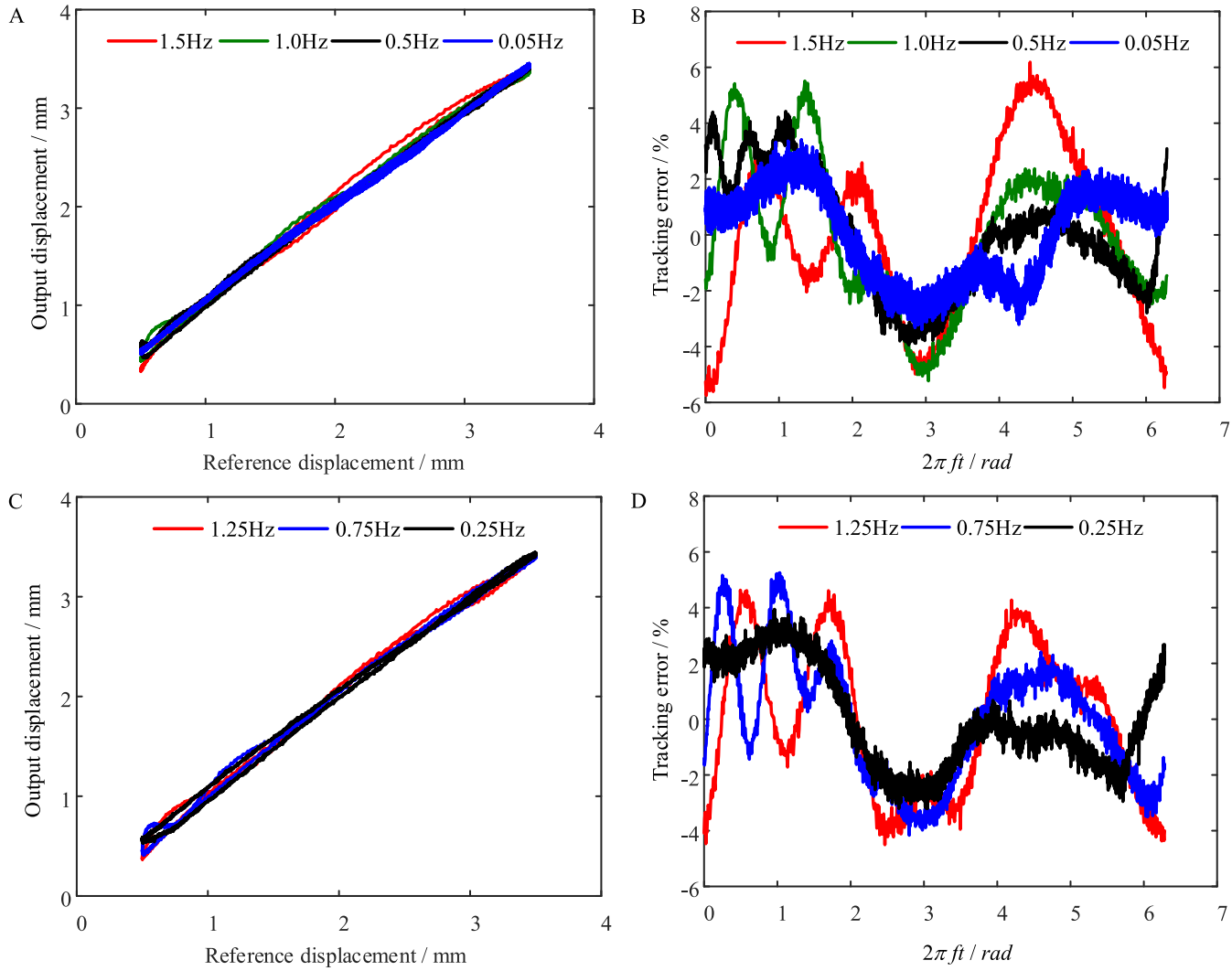

Fig. 11. Tracking experimental results with our control approach. (A) The output displacement is plotted as a function of reference displacement under the four frequencies (1.5 Hz, 1.0 Hz, 0.5 Hz and 0.05 Hz) used for the MRPIM identification. (B) Tracking errors with the four different frequencies. (C) Tracking results with other three frequencies (1.25 Hz, 0.75 Hz and 0.25 Hz). (D) Comparison of tracking errors with other three frequencies.

V. Conclusions

In this letter, we propose a feedforward control approach for rate-dependent viscoelastic hysteresis compensation of dielectric elastomer actuators. To achieve this objective, we firstly characterize the viscoelasticity of the conical dielectric elastomer actuator, which demonstrate that: i) the viscoelasticity of the dielectric elastomer actuators possess both viscoelastic creep and hysteresis nonlinearities; ii) the viscoelastic creep nonlinearity shows slow-time drift phenomenon; iii) the viscoelastic hysteresis nonlinearity is asymmetric and rate-dependent. Then, we employ a relative creep model based compensator to firstly remove the drift phenomenon. For the creep-compensated actuator, we develop a MRPIM-based direct inverse hysteresis compensator to mitigate the asymmetric and rate-dependent hysteresis nonlinearity. Various sinusoidal trajectory tracking results demonstrate that our control approach is effective to compensate for both the viscoelastic creep and rate-dependent hysteresis nonlinearities in the dielectric elastomer actuators.

References

[1] G. Gu, J. Zhu, L. Zhu, and X. Zhu, "A survey on dielectric elastomer actuators for soft robots," *Bioinspiration Biomimetics*, vol. 12, no. 1, 2017, Art. no. 011003.

[2] G. Gu, J. Zou, R. Zhao, X. Zhao, and X. Zhu, "Soft wall-climbing robots," *Sci. Robot.*, vol. 3, no. 25, 2018, Art. no. eaat2874.

[3] G. Kovacs, P. Lochmatter, and M. Wissler, "An arm wrestling robot driven by dielectric elastomer actuators," *Smart Mater. Struct.*, vol. 16, no. 2, pp. S306–S317, 2007.

[4] Y. Qiu, Z. Lu, and Q. Pei, "Refreshable tactile display based on a bistable electroactive polymer and a stretchable serpentine joule heating electrode." *ACS Appl. Mater. Interfaces*, vol. 10, no. 29, pp. 24807–24815, 2018.

[5] H. Boys, G. Frediani, S. Poslad, J. Busfield, and F. Carpi, "A dielectric elastomer actuator based tactile display for multiple fingertip interaction with virtual soft bodies," *Proc. SPIE*, vol. 10163, 2017, Art. no. 101632D.

[6] L. Calabrese, G. Frediani, M. Gei, D. De Rossi, and F. Carpi, "Active compression bandage made of electroactive elastomers," *IEEE/ASME Trans. Mechatronics*, vol. 23, no. 5, pp. 2328–2337, Oct. 2018.

[7] J. Cao *et al.*, "Untethered soft robot capable of stable locomotion using soft electrostatic actuators," *Extreme Mechanics Lett.*, vol. 21, pp. 9–16, 2018.

[8] M. Duduta, D. Clarke, and R. Wood, "A high speed soft robot based on dielectric elastomer actuators," In *Proc. IEEE Int. Conf. Robot. Autom.*, 2017, pp. 4346–4351.

[9] C. Nguyen, H. Phung, P. Hoang, T. Nguyen, H. Jung, and H. Choi, "Development of an insect-inspired hexapod robot actuated by soft actuators," *J. Mechanisms Robot.*, vol. 10, no. 6, 2018, Art. no. 061016.
[10] J. Zhao, J. Niu, D. McCoul, J. Leng, and Q. Pei, "A rotary joint for a flapping wing actuated by dielectric elastomers: Design and experiment," *Meccanica*, vol. 50, no. 11, pp. 2815–2824, 2015.
[11] E Henke, K. Wilson, and I. Anderson, "Entirely soft dielectric elastomer robots," *Proc. SPIE*, vol. 10163, 2017, Art. no. 101631N.
[12] T. Li *et al.*, "Fast-moving soft electronic fish," *Sci. Adv.*, vol. 3, no. 4, 2017, Art. no. e1602045.
[13] J. Shintake, V. Cacucciolo, H. Shea, and D. Floreano, "Soft biomimetic fish robot made of dielectric elastomer actuators," *Soft Robot.*, vol. 5, no. 4, pp. 466–474, 2018.
[14] H. Godaba, J. Li, Y. Wang, and J. Zhu, "A soft jellyfish robot driven by a dielectric elastomer actuator," *IEEE Robot. Autom. Lett.*, vol. 1, no. 2, pp. 624–631, Jul. 2016.
[15] J. Shintake, S. Rosset, B. Schubert, D. Floreano, and H. Shea, "Versatile soft grippers with intrinsic electroadhesion based on multifunctional polymer actuators," *Adv. Mater.*, vol. 28, no. 2, pp. 231–238, 2015.
[16] O. A. Araromi *et al.*, "Rollable multisegment dielectric elastomer minimum energy structures for a deployable microsatellite gripper," *IEEE/ASME Trans. Mechatronics*, vol. 20, no. 1, pp. 438–446, Feb. 2015.
[17] G. Kofod, W. Wirges, M. Paajanen, and S. Bauer, "Energy minimization for self-organized structure formation and actuation," *Appl. Phys. Lett.*, vol. 90, no. 8, 2007, Art. no. 081916.
[18] G. Gu, U Gupta, J. Zhu, L. Zhu, and X. Zhu, "Modeling of viscoelastic electromechanical behavior in a soft dielectric elastomer actuator," *IEEE Trans. Robot.*, vol. 33, no. 5, pp. 1263–1271, Oct. 2017.
[19] C. Foo, S. Cai, S. Koh, S. Bauer, and Z. Suo, "Model of dissipative dielectric elastomers," *J. Appl. Phys.*, vol. 111, no. 3, 2012, Art. no. 034102.
[20] J. Zou and G. Gu, "High-precision tracking control of a soft dielectric elastomer actuator with inverse viscoelastic hysteresis compensation," *IEEE/ASME Trans. Mechatronics*, vol. 24, no. 1, pp. 36–44, Feb. 2019.
[21] J. Zou, G. Gu, and L. Zhu, "Open-loop control of creep and vibration in dielectric elastomer actuators with phenomenological models," *IEEE/ASME Trans. Mechatronics*, vol. 22, no. 1, pp. 51–58, Feb. 2017.
[22] S. Rosset, B. O'Brien, T. Gisby, D. Xu, H. Shea, and I. Anderson, "Self-sensing dielectric elastomer actuators in closed-loop operation," *Smart Mater. Struct.*, vol. 22, no. 10, 2013, Art. no. 104018.
[23] J. Zou and G. Gu, "Modeling the viscoelastic hysteresis of dielectric elastomer actuators with a modified rate-dependent Prandtl-Ishlinskii model," *Polymers*, vol. 10, no. 5, 2018, Art. no. 525.
[24] P. Tian, W. Richard, and F. Yu, "Elliptical modelling of hysteresis operating characteristics in a dielectric elastomer tubular actuator," *Smart Mater. Struct.*, vol. 25, no. 7, 2016, Art. no. 075038.
[25] A. York, J. Dunn, and S. Seelecke, "Experimental characterization of the hysteretic and rate-dependent electromechanical behavior of dielectric electro-active polymer actuators," *Smart Mater. Struct.*, vol. 19, no. 9, 2010, Art. no. 094014.
[26] G. Gu, U. Gupta, J. Zhu, L. Zhu, and X. Zhu, "Feedforward deformation control of a dielectric elastomer actuator based on a nonlinear dynamic model," *Appl. Phys. Lett.*, vol. 107, no. 4, 2015, Art. no. 042907.
[27] G Rizzello, D Naso, A York, and S Seelecke, "Closed loop control of dielectric elastomer actuators based on self-sensing displacement feedback," *Smart Mater. Struct.*, vol. 25, no. 3, 2016, Art. no. 035034.
[28] D. Qiu, Y. Chen, and Y. Li, "Adaptive RBF neural network sliding mode control for a DEAP linear actuator," *Int. J. Performability Eng.*, vol. 13, no. 4, pp. 400–408, 2017.
[29] T. Hoffstadt and J. Maas, "Adaptive sliding mode position control for dielectric elastomer actuators," *IEEE/ASME Trans. Mechatronics*, vol. 22, no. 5, pp. 2241–2251, Oct. 2017.
[30] G. Rizzello, D. Naso, A. York, and S. Seelecke, "Modeling, identification, and control of a dielectric electro-active polymer positioning system," *IEEE Trans. Control Syst. Technol.*, vol. 23, no. 2, pp. 632–643, Mar. 2015.
[31] G. Rizzello, D. Naso, B. Turchiano, and S. Seelecke, "Robust position control of dielectric elastomer Actuators Based on LMI Optimization," *IEEE Trans. Control Syst. Technol.*, vol. 24, no. 6, pp. 1909–1921, 2016.
[32] G. Gu, M. Yang, and L. Zhu, "Real-time inverse hysteresis compensation of piezoelectric actuators with a modified Prandtl-Ishlinskii model," *Rev. Scientific Instrum.*, vol. 83, no. 6, 2012, Art. no. 065106.
[33] G. Gu, L. Zhu, C. Su, H. Ding, and S. Fatikow, "Modeling and control of piezo-actuated nanopositioning stages: A survey," *IEEE Trans. Autom. Sci. Eng.*, vol. 13, no. 1, pp. 313–332, Jan. 2016.